Physics 681: Solar Physics and Instrumentation – Lecture 14

Carsten Denker

NJIT Physics Department

Center for Solar–Terrestrial Research

Helioseismology

- Compute a solar model
- Compute the r-dependent coefficients for the oscillation PDEs
- Eigenfunctions for ξ_r, P_1, etc. and eigenfrequencies ω (non-zero solutions)
- Corrections: perfect-gas law, abundances, opacity, …
- Bring calculated eigenfrequencies in agreement with the observed frequencies (1 μHz precision, Cowling approximation is too inaccurate)
- Direct modeling: mode identification ($l = 0, \ldots, \approx 4000$ and $n \approx 35$)
- Inversion: iteration of a solar model to approximate the observed p-mode frequencies

$$\omega^2 \int \rho_0 \boldsymbol{\xi}^* \cdot \boldsymbol{\xi} dV = \int \boldsymbol{\xi}^* \left(\nabla P_1 - \frac{\rho_1}{\rho_0} \nabla P_0 + \rho_0 \nabla \Phi_1 \right) dV$$

$$= \int \rho_0 \boldsymbol{\xi}^* \cdot \mathcal{L} \xi dV$$

Sound Speed in the Solar Interior

- Dispersion relation (Duvall's law)

$$\pi\left(n+\alpha\right)/\omega=\int_{r_t}^{r_\odot}\left(\frac{1}{c^2}-\frac{l\left(l+1\right)}{r^2\omega^2}\right)^{1/2}dr$$

- Sound speed

$$\left.\begin{aligned}F\left(u\right)&=\int_u^{\xi_\odot}\left(\xi-u\right)^{-1/2}\frac{1}{r}\frac{dr}{d\xi}d\xi \ \text{ with}\\ u&=l\left(l+1\right)/\omega^2 \ \text{ and } \ \xi=\left(r/c\right)^2\end{aligned}\right\}\ \Rightarrow\ -2\frac{dF}{du}=\int_u^{\xi_\odot}\frac{dG/d\xi}{\left(\xi-u\right)^{1/2}}d\xi \ \text{ with } \ G=\ln r$$

- Abel's integral equation

$$G\left(\xi\right)-G\left(\xi_\odot\right)=-\frac{2}{\pi}\int_{\xi_\odot}^{\xi}\frac{dF/du}{\left(u-\xi\right)^{1/2}}du$$

$$\Rightarrow\ r=r_\odot\exp\left(-\frac{2}{\pi}\int_{\xi_\odot}^{\xi}\frac{dF/du}{\left(u-\xi\right)^{1/2}}du\right)$$

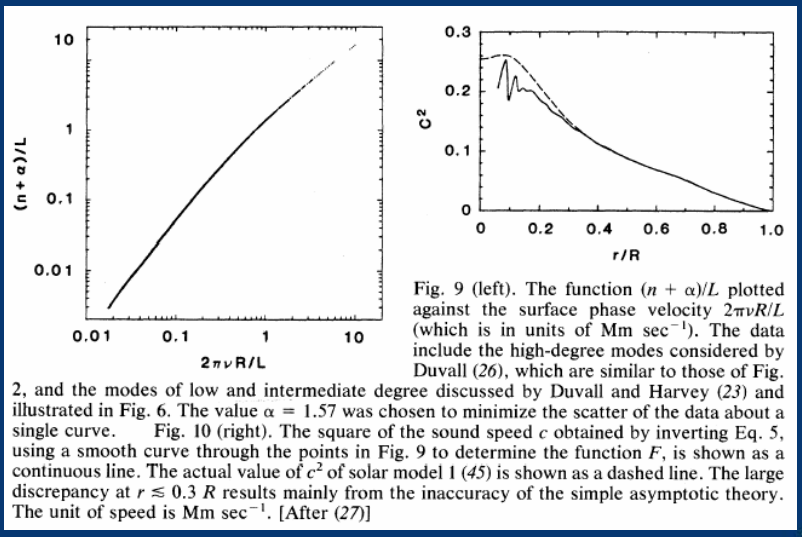

Fig. 9 (left). The function $(n + \alpha)/L$ plotted against the surface phase velocity $2\pi\nu R/L$ (which is in units of Mm sec^{-1}). The data include the high-degree modes considered by Duvall (*26*), which are similar to those of Fig. 2, and the modes of low and intermediate degree discussed by Duvall and Harvey (*23*) and illustrated in Fig. 6. The value $\alpha = 1.57$ was chosen to minimize the scatter of the data about a single curve. Fig. 10 (right). The square of the sound speed c obtained by inverting Eq. 5, using a smooth curve through the points in Fig. 9 to determine the function F, is shown as a continuous line. The actual value of c^2 of solar model 1 (*45*) is shown as a dashed line. The large discrepancy at $r \lesssim 0.3\ R$ results mainly from the inaccuracy of the simple asymptotic theory. The unit of speed is Mm sec^{-1}. [After (*27*)]

Christensen-Dalsgaard, Gough, & Toomre (1985)

Holography

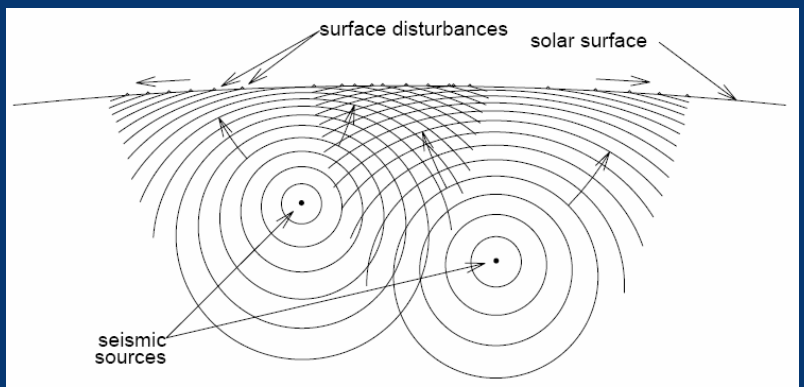

Figure 1. Seismic waves emanating from submerged sources produce surface disturbances that propagate symmetrically outward from points directly above, as indicated by arrows.

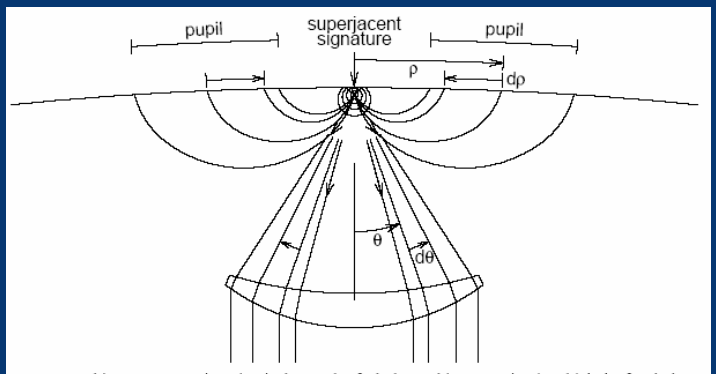

Figure 4. Subjacent vantage imaging is the result of a holographic regression in which the focal plane is shallow compared to the inner radius of the pupil. This configuration images seismic radiation that is initially emitted downward from the source and penetrates thousands of km into the solar interior before being refracted back to the surface. While the acoustic disturbance is necessarily observed at the surface, these images render the perspective of an acoustic observer looking upward into the base of the source from thousands of km beneath it. In subjacent vantage holography, the disposition of the computational pupil is substantially an inversion of that in familiar lens optics. As the angle, θ, of illumination at the focal point increases, the angular distance, ρ, along the pupil from its center, above the focal point, decreases.

Lindsey & Brown (2000)

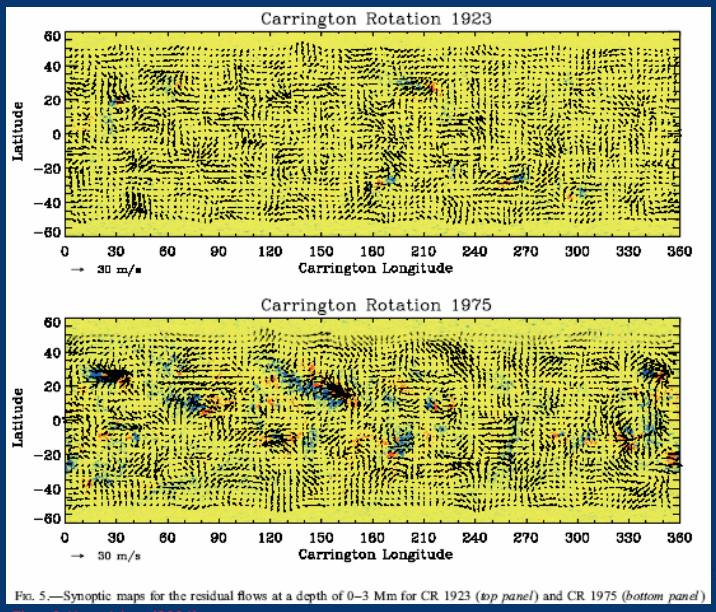

FIG. 5.—Synoptic maps for the residual flows at a depth of 0–3 Mm for CR 1923 (*top panel*) and CR 1975 (*bottom panel*)

Zhao & Kosovichev (2004)

Time-Distance Helioseismology

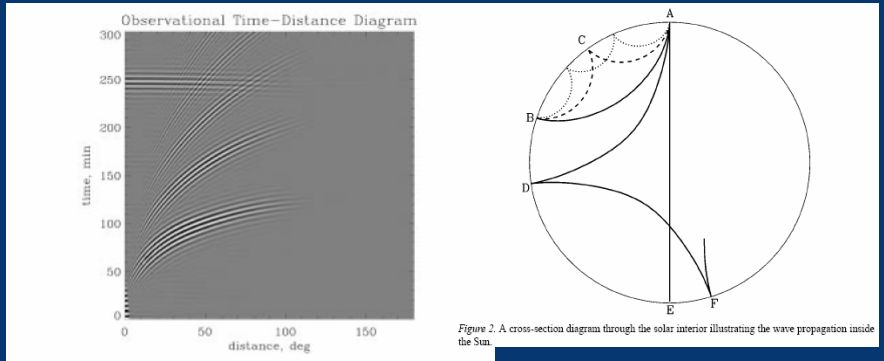

Figure 1. The observational cross-covariance function as a function of distance on the solar surface, Δ, and the delay time, τ. The lowest set of ridges ('first bounce') corresponds to waves propagated to the distance, Δ, without additional reflections from the solar surface. The middle ridge ('second bounce') is produced by the waves arriving to the same distance after one reflection from the surface, and the upper ridge ('third bounce') results from the waves arriving after two bounces from the surface. The backward ridge associated with the second-bounce ridge is due to the choice of the angular distance range from 0 to 180 deg. The correlation function was derived as the Fourier transform of the power spectrum of solar oscillations in a manner described in Duvall *et al.* (1993). The power spectrum was calculated from 144 days of MDI data starting in May 1996.

Figure 2. A cross-section diagram through the solar interior illustrating the wave propagation inside the Sun.

Kosovichev, Duvall, & Scherrer (2000)

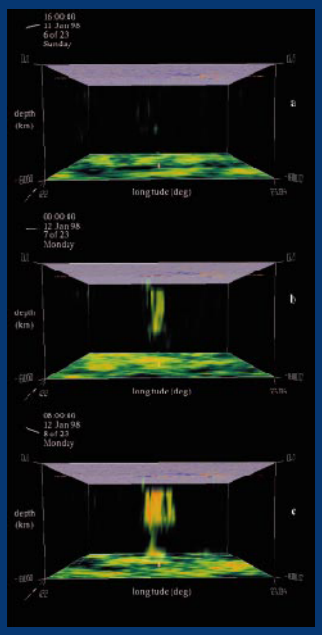
depth (km)
longitude (deg)
a
b
c

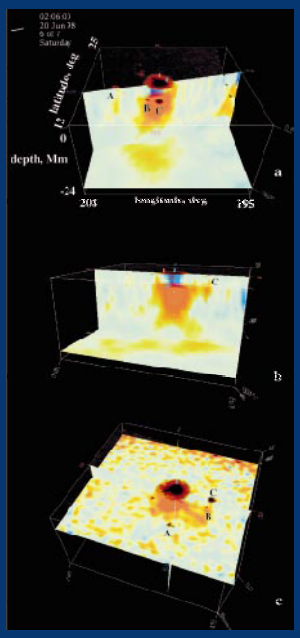
latitude, deg
depth, Mm
a
b
c